A novel three-dimensional model to quantify metastatic melanoma invasion

Cyrus M. Ghajar,[1] Vinod Suresh,[1] Shelly R. Peyton,[2] Christopher B. Raub,[1] Frank L. Meyskens, Jr.,[3,4,5] Steven C. George,[1,2] and Andrew J. Putnam[1,2,3]

Departments of [1]Biomedical Engineering, [2]Chemical Engineering and Materials Science, University of California-Irvine, Irvine, California; [3]Chao Family Comprehensive Cancer Center, Departments of [4]Medicine and [5]Biological Chemistry, University of California-Irvine School of Medicine, Orange, California

Abstract

Although attempts to develop any viable chemotherapeutic approaches to combat metastatic cancers have largely failed, potential genetic targets to halt metastatic progression continue to be identified. As drugs are developed to address these targets, there is a need for high-throughput systems that accurately reproduce *in vivo* microenvironments to gauge their efficacy. Accordingly, we have developed a three-dimensional *in vitro* culture system representative of the environment present upon secondary metastasis to quantitatively measure tumor cell invasion in this setting three-dimensionally. Culturing melanomas of different metastatic capacities within the system showed that each cell type invades the matrix in a manner commensurate to its known metastatic potential *in vivo*. Moreover, the developed quantitative schemes were put to use to characterize the effect of microenvironmental influences (i.e., matrix components, interstitial cell presence) on planar and vertical melanoma invasion. We propose this novel, quantitative system as a useful tool to assess the effects of pharmacologic and/or microenvironmental influences on tumor cell invasion at a metastatic site. [Mol Cancer Ther 2007;6(2):552–61]

Received 9/25/06; revised 11/29/06; accepted 12/21/06.

Grant support: University of California-Irvine's Council on Research, Computing and Library Resources (A.J. Putnam), setup funds from the University of California-Irvine (A.J. Putnam), and grant R01 HL067954 from the NIH (S.C. George). Partially supported by fellowships from the Achievement Rewards for College Scientists Foundation (in conjunction with the Arnold & Mabel Beckman Foundation for C.M. Ghajar) (C.M. Ghajar and S.R. Peyton).

The costs of publication of this article were defrayed in part by the payment of page charges. This article must therefore be hereby marked *advertisement* in accordance with 18 U.S.C. Section 1734 solely to indicate this fact.

Requests for reprints: Andrew Putnam, Department of Biomedical Engineering, 3120 Natural Sciences II, University of California-Irvine, Irvine, CA 92697-2715. Phone: 949-824-1243; Fax: 949-824-1727. E-mail: aputnam@uci.edu

doi:10.1158/1535-7163.MCT-06-0593

Introduction

The majority (90%) of cancer deaths arise from the spread and dissemination of a primary tumor to secondary sites of metastasis (1). This is particularly true in melanoma, an aggressive form of skin cancer responsible for 80% of all skin cancer deaths (2). The dismal 5-year survival rate of metastatic melanoma (16%; ref. 3) is troubling on two fronts: (*a*) its rising incidence; in the U.S. alone, 1 in 52 men and 1 in 73 women will develop an early stage of the disease (4); and (*b*) the absence of effective treatments; in the past 30 years, the U.S. Food and Drug Administration has approved only one drug to treat metastatic melanoma (5). Although microarray analyses continue to identify new target genes marking the progression of melanocytes to the malignant phenotype (6–9) and the contributions of the tumor microenvironment to epigenetic changes underscoring melanomagenesis continue to be elucidated (3, 10–12), the pandemic failures of current chemotherapeutic approaches (13) is distressing. Nonetheless, it is increasingly conceivable that as new targets continue to emerge, a combinatorial approach addressing a multitude of these aims will be necessary to successfully battle metastasis (5). The rapidly exploding array of experimental drugs combined with therapies aimed at the microenvironment begs for a robust, high-throughput screening tool to accurately gauge their respective effects in halting metastatic progression.

Current *in vivo* approaches to study metastasis generally involve the s.c. injection of tumor cells followed by subsequent monitoring of metastatic tumor formation at a distal site (14). Drawbacks to these approaches include the length of time required of most experiments, cost (compounded as the number of conditions increases), and the inability to monitor crucial phases of the metastatic process (14, 15). Conversely, *in vitro* models developed to study metastatic invasion, largely consisting of modified Boyden-like assays (16, 17), are intended to model the invasion of the primary tumor rather than the invasion and growth of tumor cells as they ''set up shop'' at a secondary site. The dearth of *in vitro* culture systems that recreate this process further substantiates the need for a model of secondary metastasis.

To address this void, our group has adapted a previously published three-dimensional fibrin-based model of angiogenesis (18) to develop a culture system representative of melanoma invasion at the site of extravasation. A highly metastatic melanoma cell line (C8161.9), a cutaneous melanoma cell line (M14), and human epidermal melanocytes of neonatal origin (HEMn) were coated on microcarrier beads and polymerized within fibrin or fibrin-collagen hydrogels. A layer of dermal fibroblasts (DF) was added to more accurately simulate the microenvironment. Invasion of each cell type was monitored over a 7-day period

and quantified via novel methods developed to assess their planar and vertical invasion. The results show that each cell type invades the matrix in a manner commensurate to its established metastatic capacity *in vivo* and, curiously, seem to recapitulate their *in situ* growth patterns (i.e., those that take place in architecturally defined skin). Experiments also shed some light on the role of fibrin and fibroblasts in metastatic melanoma invasion. Results from these experiments validate the system to quantitatively gauge the effect of microenvironmental influences on metastatic tumor cell invasion and establish its potential as a high-throughput screening tool to assess the efficacy of pharmacologic inhibitors targeting metastatic forms of cancer.

Materials and Methods

Fibrin Tissue Construction

Cytodex-3 microcarrier beads (Sigma-Aldrich, St. Louis, MO), spherical (mean diameter ≈ 170 μm) dextran beads coated with denatured collagen to facilitate cell adhesion, were coated with either C8161.9 melanoma cells, M14 melanoma cells (both cell lines a generous gift from Cindy Miranti, Van Andel Institute, Grand Rapids, MI), or HEMn-moderate pigmentation (Cascade Biologics, Portland, OR, used before passage 5) as follows: 4 million cells were mixed with 10,000 Cytodex beads immersed in 5 mL of media within an upright T-25 culture flask. The flask was gently agitated every half hour to ensure that the cells coated the beads ubiquitously. After 4 h, beads were transferred to a new T-25 flask situated in its normal cell culture position, and 5 mL of fresh media was added.

The following day, cell-coated beads were mixed at a concentration of 50 beads/mL within a 3-mg/mL fibrinogen solution [bovine fibrinogen (Sigma) dissolved in PBS (pH, 7.4)]. For collagen-containing conditions, 10% (by weight) type I collagen (BD Biosciences, San Jose, CA) was added to a fibrinogen solution with a slightly higher starting concentration to compensate for the subsequent dilution by collagen addition. Then, 0.5 mL of either solution was mixed with 10 μL of a 50 units/mL solution of thrombin (Sigma) within a 24-well plate. After allowing tissues to clot at room temperature for 5 min, well plates were transferred to a cell culture incubator (37°C, 5% CO_2) for an additional 20 min. Finally, for DF-containing conditions, fibrin tissues were overlaid with DF (American Type Culture Collection, Manassas, VA; used before passage 10) at a concentration of 25,000/mL within either DMEM-F12 (Invitrogen, Carlsbad, CA) supplemented with 5% fetal bovine serum and 1% of the following: sodium-pyruvate, non–essential amino acids, penicillin-streptomycin, and L-glutamine (all from Invitrogen; for C8161.9 and M14) or Medium 254 (Cascade Biologics) supplemented with human melanocyte growth supplement (for HEMn). For DF-absent conditions, tissues were overlaid with their respective growth mediums. Media was changed at day 1 and every other subsequent day.

Image Acquisition and *X-Y* Invasion Quantification

Tissues were imaged via bright-field phase-contrast microscopy with a Nikon TE300 microscope (Nikon, Melville, NY) at three time points postassembly: days 1, 3, and 7 (Fig. 1). At least seven isolated beads per condition (beads lacking any neighbors within one field of view in any direction at a low magnification setting) were randomly located per condition at day 1. The coordinates of each bead were recorded (in reference to a randomly selected origin within each 24-well plate, which was noted and located again at each subsequent time point), and beads were tracked and imaged over the time course of the experiment using Metamorph software (Universal Imaging/Molecular Devices Corporation, Union City, CA). Beads were imaged at low power (4×) using a negative phase-contrast objective. The resulting images were then saved as high-resolution files (*.tif).

These files were then subjected to the fully automated image processing modality illustrated in Fig. 2 using NIH ImageJ open source software (NIH, Bethesda, MD) to quantify invasion into the surrounding matrix. Low-magnification images (Fig. 2A) were first sharpened (Fig. 2B) to enhance contrast and accentuate detail. The ''find edges'' function was then performed (Fig. 2C) to further highlight sharp changes in intensity between neighboring pixels. This additional step seemed to aid the autothreshold function (Fig. 2D); when applied, this function segmented the image into features of interest (in this case, the brighter cell populations, *red*) and background (*black* or *gray*). To quantify the total area occupied by cells, the thresholded areas were traced (Fig. 2E), and the sum of the areas occupied by these traced objects (reflected in Fig. 2F) was totaled (image clusters consisting of less than 10 pixels were ignored to account for noise). The result was a metric for percent invasion, which is the total percentage of the low magnification field of view occupied by a population of cells emanating from a single source, in this case, a microcarrier bead. It is important to note that all described steps are automated features of ImageJ and required no subjective input from the user.

Labeling of Cells via Green Fluorescent Protein Adenovirus

Green fluorescent protein (GFP) recombinant adenoviruses were packaged using a modified protocol for the AdEasy XL system (Stratagene, La Jolla, CA). Briefly, linearized plasmids (a generous gift from Christopher Chen, University of Pennsylvania, Philadelphia, PA) were used to transfect HEK293 cells (American Type Culture Collection) with LipofectAMINE Plus (Invitrogen) according to manufacturer's instructions. High titer preparations of the resulting adenovirus were extracted from the cells by repeated freeze-thaw using liquid nitrogen and 37°C water baths. The virus was then cleared by centrifugation and purified with a cesium chloride ultracentrifugation gradient. Viral infection efficiency was empirically determined by serial dilutions using each cell type in question and observing the GFP fluorescence from 24 h to 8 days. In GFP

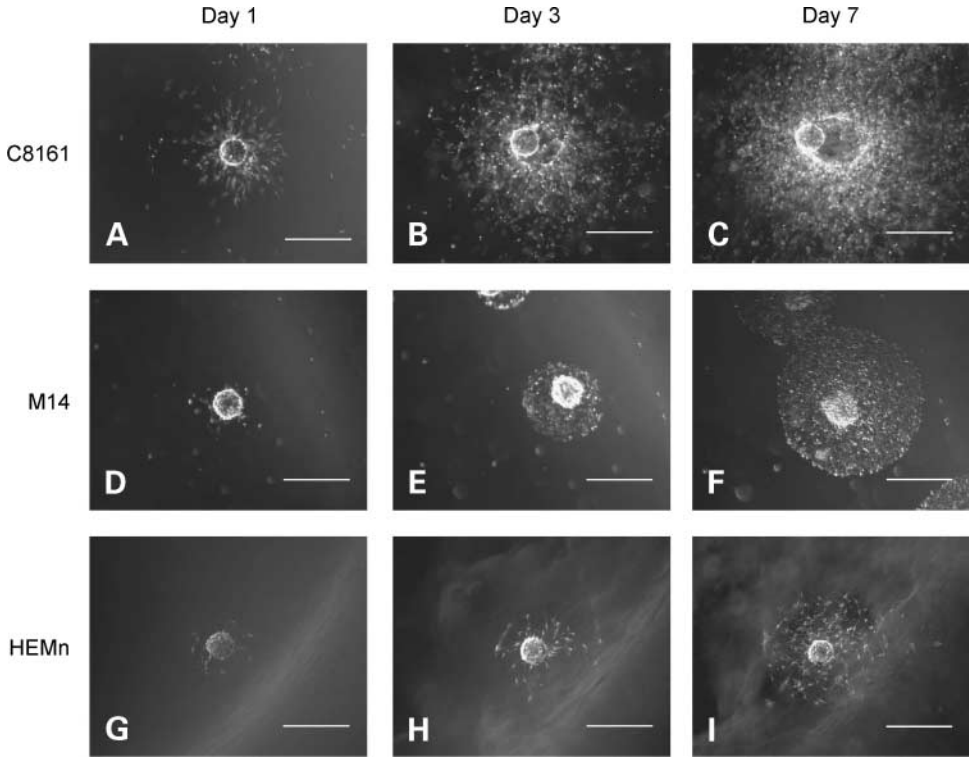

Figure 1. HEMn, M14s, and C8161s recapture their *in vivo* phenotypes when cultured within three-dimensional fibrin gels. C8161s (**A – C**), M14s (**D – F**), and HEMn (**G – I**) cultured within 3.0 mg/mL fibrin hydrogels and tracked from day 1 (**A, D,** and **G**) through day 7 (**C, F,** and **I**). Bars, 500 μm.

infection experiments, viral multiplicity of infection resulting in a transduction efficiency of at least 80% (3.4 μg viral multiplicity of infection per milliliter of bead suspension for C8161s and M14s; 2.55 μg/mL for HEMn) was added to cell-dextran bead suspensions for 24 h. At this time, the media was removed, and beads were twice washed and incorporated into fibrin gels as described above.

Confocal Imaging of Vertical Invasion

Invasion in the *Z*-plane was assessed at day 7 using a Zeiss LSM 510 Meta (Carl Zeiss, Germany). For each condition, beads coated with GFP-infected cells were focused on with a 10× objective and excited with a 488-nm laser. *Z*-stack parameters were set such that imaging would begin 500 μm below the bead and end 1,000 μm above the bead, scanning image planes every 50 μm (31 images total). This range was found to encompass the maximum distance traversed by cells in the *Z*-direction across all conditions. The pinhole size was set such that the overlap of fluorescence between neighboring planes would be minimal.

The 31 images comprising a *Z*-stack were then combined and stacked using LSM Image Browser software (Carl Zeiss) to generate a three-dimensional projection. This projection was then rotated about the *Y*-axis (as depicted atop Fig. 5) by 90° to view invasion throughout the 1.5-mm depth of the entire stack. Once rotated, images were autothresholded in a binary fashion. The percentage of the total image area occupied by the thresholded region was quantified to yield a percent vertical invasion using NIH ImageJ.

Statistical Analyses

Statistical analyses were done using InStat 2.01. Data are reported as mean ± SD. All statistical comparisons were made by performing a one-way ANOVA, followed by a Student-Newman-Keuls multiple comparisons test to judge significance between two data sets at a time. P values <0.05 were considered statistically significant.

Results

Cells of Melanocytic Origins Recapture Their *In situ* Phenotypes When Cultured within Three-Dimensional Fibrin Hydrogels

C8161.9, a highly metastatic subclone (19) of a line of melanoma cells originally established by Bregman and Meyskens (20), were coated onto Cytodex microcarrier beads and polymerized within 3.0 mg/mL fibrin hydrogels overlaid with a DF monolayer. These cells were highly invasive when tracked over a 7-day period (Fig. 1). The observed phenotype was consistent with their established *in vivo* behavior (21). Relatively aggressive invasion was evident within 24 h (Fig. 1A), whereas a more well-defined invasive front became apparent after 3 days (Fig. 1B) and continued to grow through day 7 (Fig. 1C). The majority of cells continued to proliferate and invade from this central pocket.

A cell line derived from a primary melanoma (M14; ref. 22) was also cultured within the system to contrast with the invasion displayed by the highly metastatic C8161.9. The sporadically metastatic M14 assumed a coordinated

form of invasion (Fig. 1D–F) that contrasted sharply to that of C8161.9. Although these cells typically formed an invasive front as well by day 3 (Fig. 1E), individual populations of cells did not deviate from the central cluster, restricting their invasion to a symmetrical, apparently planar mode.

Normal melanocytes (HEMn) were also cultured within this system to assess whether it was appropriate as a model of invasion at a metastatic site. When grown in media identical to that of the C8161.9 and M14, HEMn seemed to lack any invasive/migratory capacity (data not shown). As a result, HEMn were instead cultured in media specialized for melanocyte growth. Although specialty media stimulated HEMn migration into the matrix, invasion did not seem coordinated over the 7-day period (Fig. 1G–I). Moreover, HEMn maintained their polarized, spindle-like appearance over the course of the experiment.

An Image Processing Approach Was Developed to Quantify Planar Invasion of Cells into Their Surrounding Matrix

Based on the results presented in Fig. 1, it was evident that the development of a quantitative scheme was necessary to determine the statistical significance of the observed differences in invasion of each cell type and the effects of any subsequent manipulations to experimental conditions (e.g., microenvironmental changes or addition of pharmacologic inhibitors). Figure 2 illustrates the automated steps developed using NIH ImageJ to define the percentage of the total field of view occupied by a single population of cells (i.e., those originating from a single, isolated bead) at any discrete time point.

A low-magnification (4×) image (Fig. 2A) of an isolated bead was sharpened (Fig. 2B) and had its edges accentuated (Fig. 2C) to define differences in intensity of neighboring pixels. These steps were found to reduce noise when autothresholding the image (Fig. 2D) into its binary form. Once the image was translated into binary form, a tracing function of the image processing software was used to outline the clusters of pixels (Fig. 2E) exceeding the threshold limit (Fig. 2D, *red*). The areas encompassed by these discrete closed loops (Fig. 2F) were tallied to produce the metric of ''percent invasion.'' This percentage reflects the fraction of the total pixel area of an image occupied by a population of cells invading from a single, isolated bead.

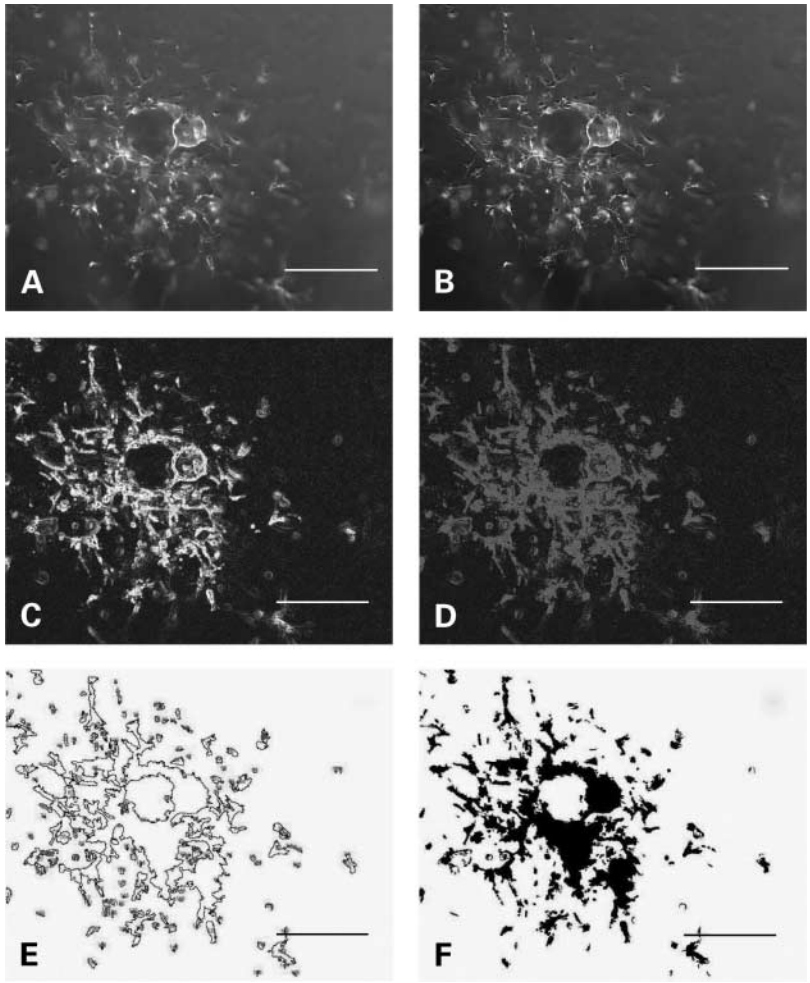

Figure 2. A quantitative imaging method to assess radial invasion. To quantify invasion into the surrounding matrix by each cell type investigated, (**A**) low-magnification images of isolated beads were sharpened (**B**), edges were defined (**C**), and thresholded (**D**). *Red*, cells or cell clusters. These thresholded regions were traced (**E**), and the area occupied by these thresholded areas (**F**) was finally calculated and summed to yield a percentage of the total image area occupied by cells. The end result is a metric for the percent invasion of each cell type.

Quantifying Planar Invasion Reveals That M14s Are the Only Cell Type Affected by DF Presence within Fibrin Matrices

To better characterize the model system, the effect of including DF was assessed by applying the described quantitative scheme to C8161.9, M14, and HEMn invasion in the presence or absence of a DF monolayer. Although there was little phenotypic difference observed among the C8161.9 cultures (Fig. 3A and D) or HEMn cultures (Fig. 3C and F), M14 outgrowth (Fig. 3B and E) was dramatically affected by the removal of the DF monolayer. M14 deviated from their symmetrical, coordinated invasion in the presence of the DF monolayer by assuming a morphology akin to C8161.9 when cultured in a DF-absent environment. These qualitative observations were confirmed through the developed quantitative approach. With the DF monolayer present, C8161.9 were significantly more invasive than M14 or HEMn as early as day 1, culminating by day 7 to be nearly thrice more invasive than M14s (45.74 $\pm$ 4.04% versus 16.06 $\pm$ 4.42%). Meanwhile, M14 invasion was over double that of HEMn invasion by day 7 (16.06 $\pm$ 4.42% versus 7.33 $\pm$ 0.75%). As anticipated, removing DF did not significantly affect the extent of C8161.9 or HEMn invasion. However, a significant increase in M14 invasion between these conditions was observed as early as day 3; M14 invasion without the DF monolayer reached the level of C8161.9 (9.09 $\pm$ 2.59 for C8161.9 versus 9.49 $\pm$ 3.55 for M14) from this point on.

The Addition of Collagen Slows the Invasion of All Cell Types with DF Present by Day 7

To better represent the tumor microenvironment (23, 24), collagen (10% by weight) was polymerized within the fibrin matrices. Comparing results from these experiments with those conducted in a pure fibrin matrix (Fig. 3) hints at the notion that fibrin may function to accelerate invasion within the metastatic microenvironment. The addition of collagen significantly reduced the invasion within all cultures containing DF by day 7 compared with cultures containing pure fibrin; C8161.9 invasion was reduced by 35%, M14 invasion was reduced by 75%, and HEMn invasion was reduced by 69%. Among conditions lacking DF, M14 and HEMn invasion were significantly reduced by day 7.

Trends in collagen-containing matrices also deviated from those established in the purely fibrin cultures. With DF present, C8161.9 displayed a significantly higher percent invasion than M14 or HEMn from day 1 onward. However, M14 cultured in this condition did not invade significantly more than did the HEMn at any time point (Fig. 4G). C8161.9 invasion increased with the removal of DF (Fig. 4 A, D, and G) by day 7 within the fibrin-collagen matrices (29.60 $\pm$ 8.73% versus 54.06 $\pm$ 11.12%), as did M14 invasion (Fig. 4B, E, and G), which experienced a nearly 6-fold increase in percent invasion (4.09 $\pm$ 1.89% versus 22.6 $\pm$ 9.23%) upon DF removal by day 7. M14 invasion again seemed to proceed in a disorganized fashion (Fig. 4E), lacking the invasive front present in conditions containing the DF monolayer (Fig. 4B).

C8161.9, M14, and HEMn Recapitulate Epidermal Growth Patterns When Cultured within Three-Dimensional Fibrin or Fibrin-Collagen Matrices

Although it is widely appreciated that the transition from radial growth phase to vertical growth phase is a critical aspect of melanomagenesis *in situ* (25), it is not clear

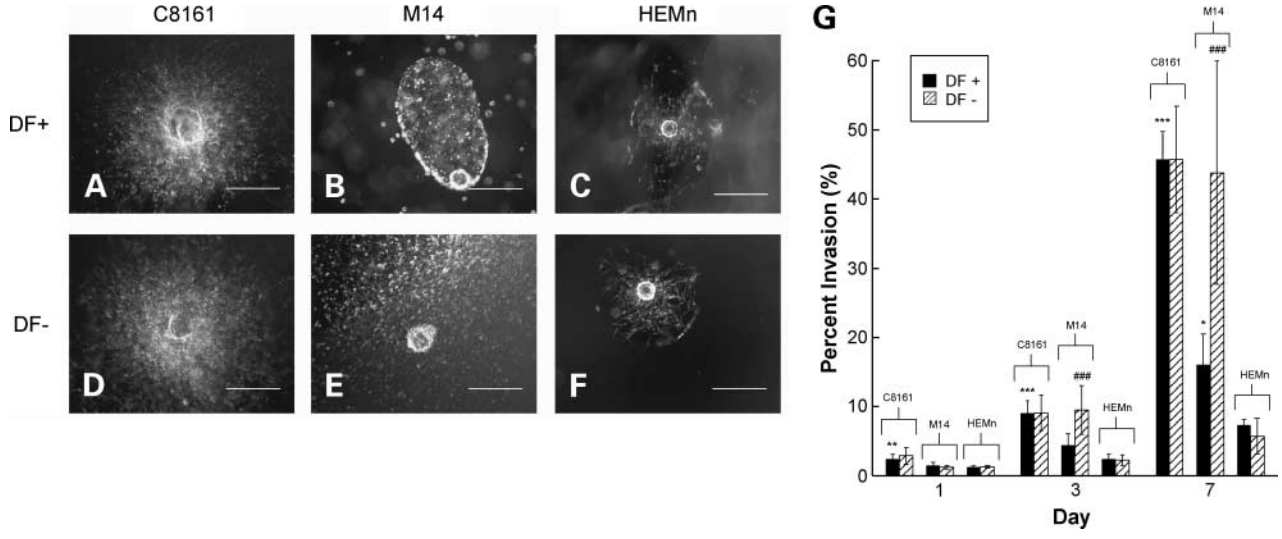

Figure 3. Quantifying radial invasion reveals that M14s are the only cell type affected by DF presence within fibrin matrices. Representative day 7 images of C8161 (**A** and **D**), M14 (**B** and **E**), and HEMn (**C** and **F**) cultured within 3.0 mg/mL fibrin matrices in the presence (**A**–**C**) or in the absence (**D**–**F**) of a DF monolayer. Bars, 500 μm. At three separate time points (days 1, 3, and 7), seven images per condition were acquired and processed using the modality described in Fig. 2. The resulting percent invasion for each condition was averaged and compared as presented in **G**. *, $P < 0.05$ when comparing M14 invasion to HEMn invasion at day 7. **, $P < 0.01$ when comparing C8161 invasion to M14 and HEMn invasion at day 1. ***, $P < 0.001$ when comparing C8161 invasion to M14 and HEMn invasion at days 3 and 7. $^{\#\#\#}$, $P < 0.001$ when comparing DF+ to DF− conditions for M14 cultures at days 3 and 7.

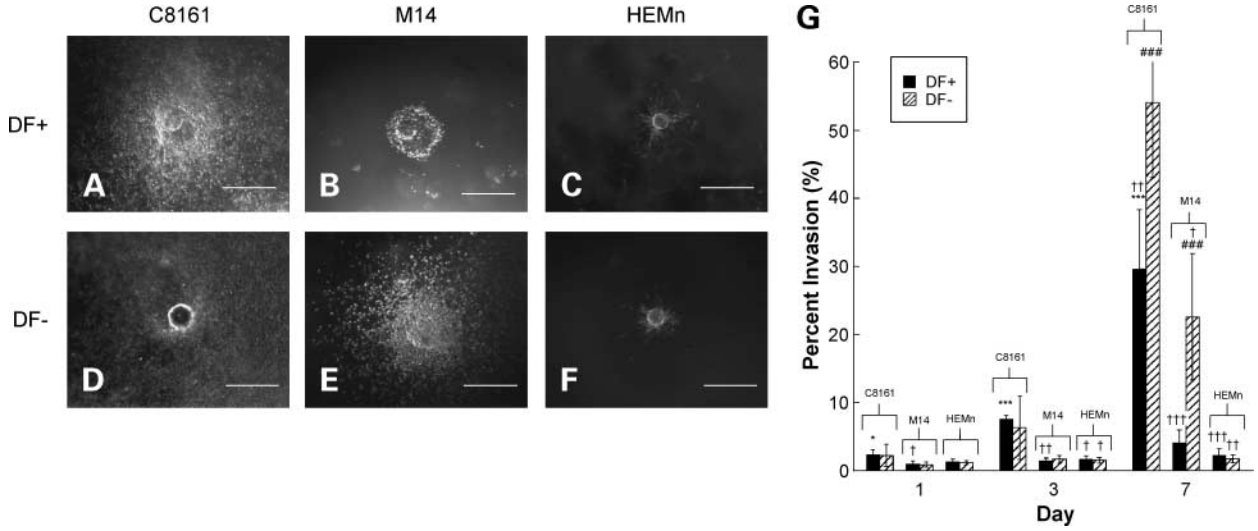

Figure 4. Quantifying radial invasion within fibrin-collagen matrices shows that the addition of collagen slows the invasion of all cell types by day 7. Representative day 7 images of C8161 (**A** and **D**), M14 (**B** and **E**), and HEMn (**C** and **F**) cultured within 3.0 mg/mL fibrin – 10% collagen I matrices in the presence (**A** – **C**) or in the absence (**D** – **F**) of a DF monolayer. Bars, 500 μm. At three separate time points (days 1, 3, and 7), seven images per condition were acquired and processed using the modality described in Fig. 2. The resulting values of the percent invasion for each condition were averaged and compared as presented in **G**. *, $P < 0.05$ when comparing C8161 invasion to M14 and HEMn values at day 1. ***, $P < 0.001$ when comparing C8161 invasion to M14 and HEMn invasion at days 3 and 7. ###, $P < 0.001$ when comparing DF+ and DF− conditions of C8161 or M14 cultures at day 7. †, significance in an identical fashion when comparing either condition and time point to its corresponding condition and time point in Fig. 3 (i.e., † †, facilitate comparison between identical conditions and time points between pure fibrin matrices and fibrin-collagen matrices).

whether each cell type would retain these radial versus vertical invasion characteristics at a site of secondary metastasis. To address this question, microcarrier beads were coated with GFP-infected cells and cultured within fibrin or fibrin-collagen matrices in the presence or absence of DF. Cultures were imaged every 50 μm over a depth of 1.5 mm via confocal microscopy, and the resulting *Z*-stacks were compiled to generate three-dimensional projections of vertical invasion (see illustration atop Fig. 5).

Strikingly, C8161.9 (Figs. 5A and B and 6A and B) displayed extensive invasion throughout the *Z*-axis, whereas M14 invasion (Figs. 5C and D and 6C and D), by and large, remained planar. Binary thresholding and quantification of the area occupied by each cell type (Figs. 5G and 6G) in the vertical plane of either condition revealed that C8161.9 occupied over 30% of these planes, thrice that of M14s in each case. The addition of collagen, while reducing planar invasion, significantly enhanced the vertical invasion of both C8161.9 and M14 in the presence of DF when compared with the corresponding condition in pure fibrin (Fig. 6G).

In the absence of DF, vertical invasion of HEMn proceeded as expected. HEMn deviated very little from their radial growth plane in fibrin (Fig. 5F) or fibrin-collagen (Fig. 6F) matrices. However, once cultured in the presence of DF, melanocytes acquired some verticality to their invasion (Figs. 5E and 6E). Quantification revealed a significant increase in the percent of vertical invasion when DF were included in the fibrin-collagen matrices; vertical invasion increased from 8.88 ± 0.65% (DF−) to 15.21 ± 1.41% (DF+) in these matrices.

Discussion

The majority of *in vivo* models of metastasis determine the effect of experimental conditions (usually via knock-out mice) by relying on the end point of secondary tumor formation at a distal site (14). However, the steps occurring between tumor cell injection and metastatic tumor formation are effectively shrouded in these models (15). Despite advances in imaging to monitor these processes, a crucial step of metastasis—the invasion and colonization of cancer cells upon extravasation—remains an elusive target. This study describes a three-dimensional culture system developed to model this phase *in vitro* and establishes the efficacy of this novel system by demonstrating that cells from disparate phases of melanoma invade the matrix in a manner proportional to their known metastatic capabilities. Specifically, the highly metastatic C8161.9 stayed true to its documented *in vivo* behavior (21), ferociously staking claim to much of the surrounding matrix (Fig. 1A–C). The sporadically metastatic M14 invaded the matrix far less extensively than their highly metastatic counterparts (Fig. 1D-F) and did so in a coordinated and symmetrical fashion reminiscent of collective cell migration (26). This feature of M14 invasion may underlie its less aggressive nature when compared with C8161.9, which seem to migrate individually. Conversely, the untransformed HEMn did not extensively invade the matrix (Fig. 1G-I), even when cultured in specialty medium. Moreover, HEMn retained their polarized, spindle-like morphology despite the unfamiliar surroundings of a fibrin-rich matrix. This ability to judge morphologic differences between cell lines of the same

cancer type is a strength of this system, providing a potential end point to measure the effects of experimental conditions.

Perhaps the most useful aspect of this system is the ability to quantitatively track the planar and vertical invasion of any cell type in the long term (Figs. 2 and 5). In the present context, this feature of the system led to a number of interesting and potentially useful observations regarding effects of the microenvironment on metastatic invasion. The first is that it elucidated a potential role of fibrin in the metastatic process that has previously been overlooked. Fibrin has been shown to enhance metastatic potential of tumor cells (27) through a combination of functions, including the enhancement of tumor cell binding to platelets (28) and adhesion to the vasculature of target organs (27) before extravasation. However, the role fibrin plays at the site of secondary metastasis, where it ostensibly is secreted into the interstitium as metastatic cells extravasate and then coagulates around the preexisting, primarily type I collagen extracellular matrix (29), is undefined. Metastatic C8161.9 and M14 each showed relatively moderate growth in collagen-containing matrices in the presence of fibroblasts (Fig. 4A and B). However, in pure fibrin matrices (Fig. 3A and B), C8161.9 and M14 each displayed enhanced invasion. C8161.9 invasion was increased by 55%, whereas M14 invasion increased nearly 4-fold (Figs. 3G and 4G). This provides causal evidence that, in addition to its known functions to abet metastasis, fibrin may enhance the migratory and invasive capacities of metastatic cells.

Another quantifiable observation was that the presence of fibroblasts in the model system curtailed the invasion of tumor cells. For instance, in the fibrin-collagen matrices, C8161.9 invasion increased by nearly 83%, whereas migration of M14 became individual-cell dominant, and invasion nearly quintupled with the removal of the DF

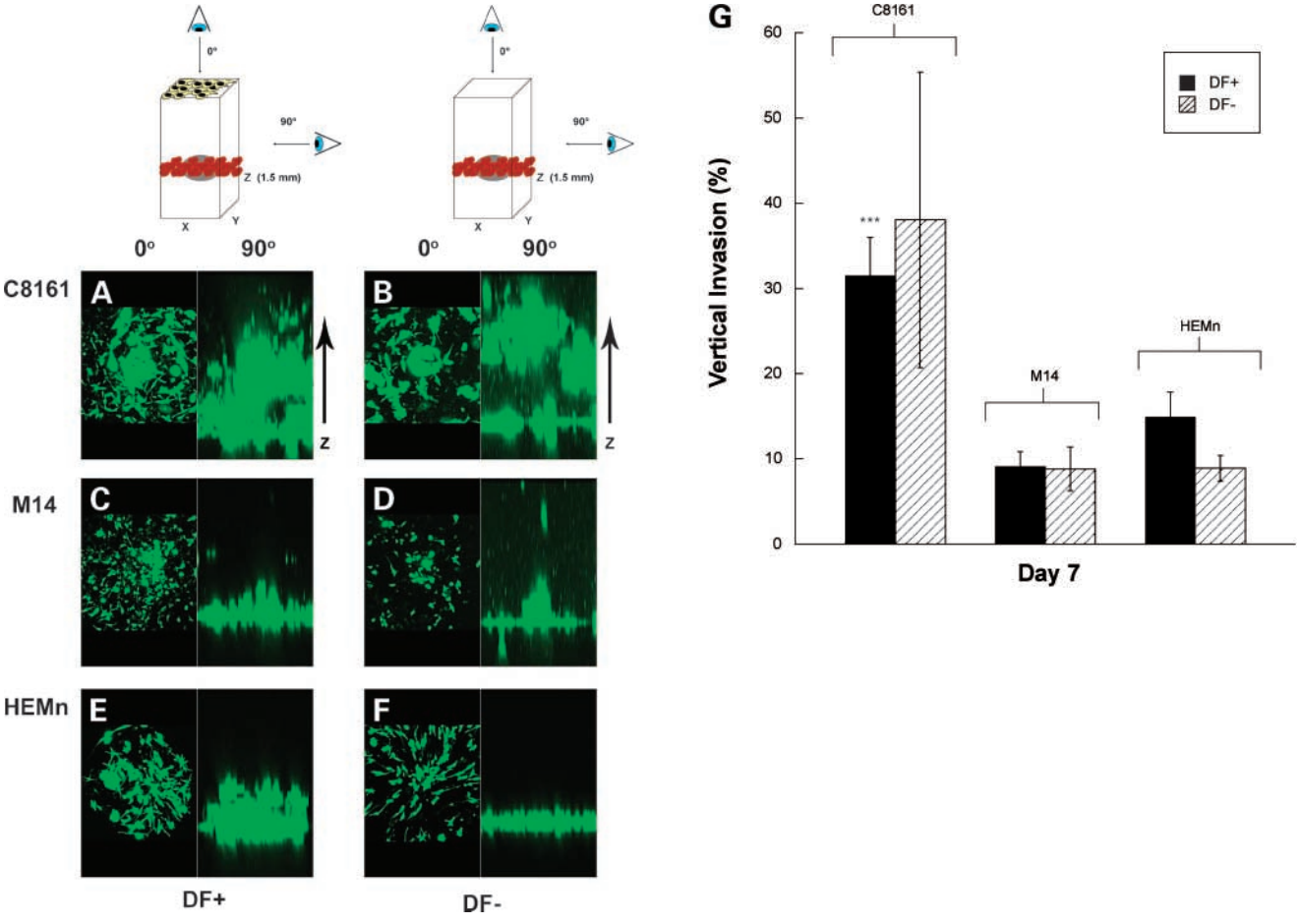

Figure 5. Although characteristic of a metastatic environment, C8161, M14, and HEMn recapitulate their *in situ* growth patterns when cultured in three-dimensional fibrin matrices. Confocal *Z*-stacks were acquired for each condition and projected three dimensionally. For each condition: *left,* a representative view from the top of this projection; *right,* the view after rotating this projection 90° about its *Y*-axis (as depicted in the schematic at the *top*). Representative day 7 projections of GFP-infected C8161 (**A** and **B**), M14 (**C** and **D**), and HEMn (**E** and **F**) invading 3.0 mg/mL fibrin matrices in the presence (**A**, **C,** and **E**) or in the absence (**B**, **D,** and **F**) of a DF monolayer. Five images per condition were thresholded and quantified to yield a percent vertical invasion. The resulting values for each condition were averaged and compared as presented in **G**. ***, $P < 0.001$ when comparing vertical invasion of C8161 (DF+) to that of M14 and HEMn.

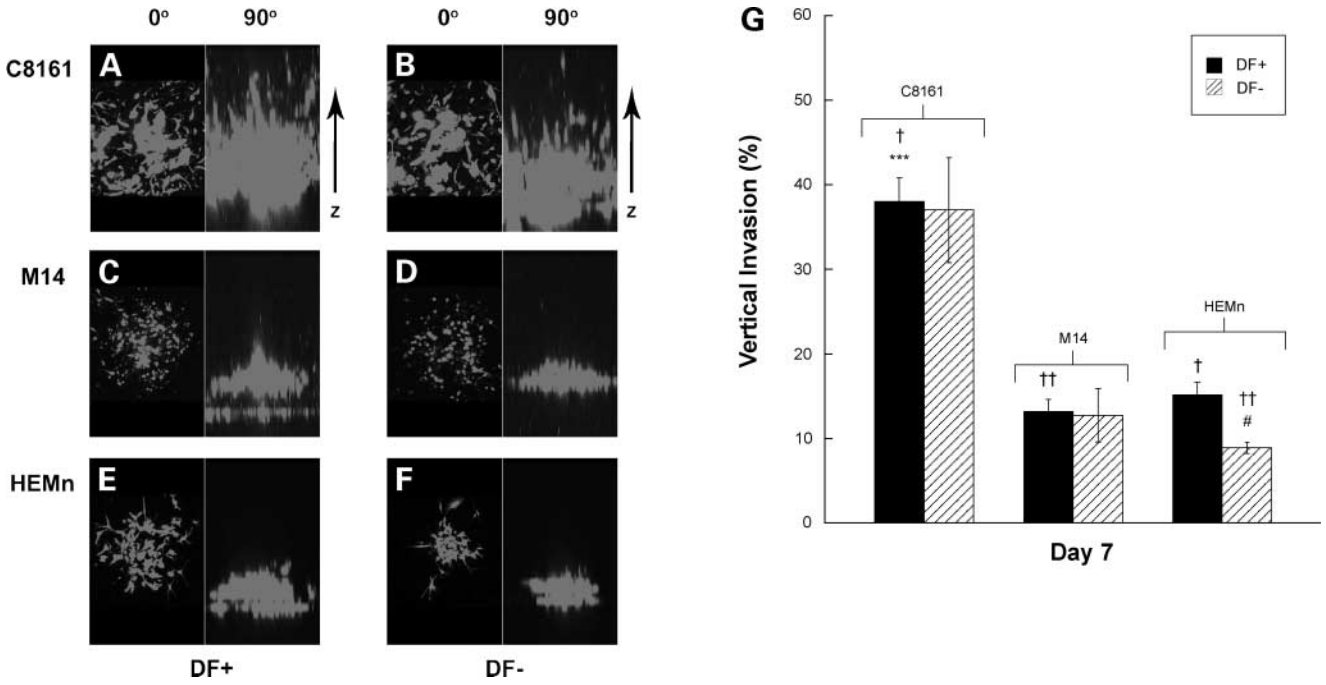

Figure 6. The addition of collagen largely encourages vertical invasion of all cell types when compared with pure fibrin matrices. Representative day 7 projections (as described in Fig. 5) of GFP-infected C8161 (**A** and **B**), M14 (**C** and **D**), and HEMn (**E** and **F**) invading 3.0 mg/mL fibrin – 10% collagen matrices in the presence (**A**, **C**, and **E**) or in the absence (**B**, **D**, and **F**) of a DF monolayer. Five images per condition were thresholded and quantified to yield a percent vertical invasion. The resulting values for each condition were averaged and compared as presented in **G**. ***, $P < 0.001$ when comparing vertical invasion of C8161 (DF+) to that of M14 and HEMn. #, $P < 0.05$ when comparing vertical invasion of DF+ and DF− conditions of HEMn cultures. †, significance in an identical fashion when comparing either condition to its corresponding condition and in Fig. 5 (i.e., ††, facilitate comparison between identical conditions between pure fibrin matrices and fibrin-collagen matrices).

monolayer (Fig. 4G). These results are somewhat paradoxical given the established function of fibroblasts in enhancing tumor growth and invasion (30), generally, and that of melanoma (31), specifically. However, it is important to note that the inhibitory effect of both DF presence and collagen addition on melanoma invasion in the context of a fibrin matrix may be due to reduced proteolysis caused by these alterations. In particular, fibrin can be cleaved by the cell-secreted protease plasmin, resulting in a number of degradation products. Among these, the fibrin E-fragment (consisting of the NH_2-terminal regions of the three distinct fibrin chains held together by disulfide bonds; ref. 32) and degradation product complexes containing this fragment have been shown to dramatically increase the activation of plasmin from its zymogen plasminogen and, hence, the proteolysis of fibrinogen (33). Accordingly, it is possible that factors secreted by DF interfere with the production of these fragments and potentiate plasmin activation to a lesser degree. Furthermore, collagen I has been shown to promote plasmin activation to a lesser degree than fibrin alone (34). The ultimate result of the subsequent reduction in available plasmin could very well be observed reduction in melanoma invasion. Nonetheless, the present study provides precursory evidence that fibrin may enhance melanoma invasiveness, whereas fibroblasts not only do not enhance, but may in fact restrict, invasion at the metastatic site. The ultimate effects of these components on metastatic progression are potential topics of future investigation.

The final interesting feature captured in this model system relates to the vertical invasion of C8161.9, M14, and HEMn, assessed by confocal sectioning of the GFP-infected forms of each cell type (Figs. 5 and 6). Despite being placed in a microenvironment not representative of architecturally defined, collagen-rich skin (modeled well in human skin reconstructs; ref. 35), the invasion of the investigated cell types faithfully recapitulated their *in situ* vertical growth patterns. Aberrant melanocytes escape keratinocyte control of proliferation, form nevi, and develop dysplasia (precancerous lesions) and hyperplasia (dramatic increases in cell number) in the epidermis, defining radial growth phase melanoma. Progression to the vertical growth phase involves the penetration of an underlying basement membrane into the dermal layer (36). Within the present culture system, vertical invasion of untransformed HEMn and sporadically metastatic M14 remained planar, or ''radial.'' Meanwhile, C8161.9 migrated extensively either toward the DF monolayer or, in the absence of the monolayer, toward the nutrient source (culture medium). Although the vertical invasion of M14 did not depend on the presence of DF, remaining largely planar in either case,

the vertical growth of HEMn did seem to be affected by DF in collagen-containing matrices. This enhancement occurred despite the lack of melanocyte-DF contact, hinting that it may be solely mediated by DF-secreted factors. These data provide interesting new evidence suggesting that, whereas the microenvironment may influence the aberrant growth of melanoma in the skin, a ''minimum functional unit'' may exist within the *in vitro* microenvironment, which signals the cells to follow their *in situ* growth patterns. Perhaps simply culturing the cells within a matrix accomplishes this as culturing tumor cells in three dimensions has led to the recapitulation of *in vivo* behaviors of a variety of cancer cell types (37–39). Nevertheless, given that vertical invasion is required for metastasis (25), assessing the depth of vertical penetration may provide another prognostic tool to evaluate the effectiveness of therapies in reducing the metastastic capacity of melanoma cells within this model.

A robust *in vitro* system must allow the investigated process to occur in the context of a natural surrounding, facilitate manipulations of both the cells and the microenvironment, be easy to perform, and have an easily evaluated end point (40). The system described herein contains each of these ingredients. A particular strength is that it allows for a wealth of variables to probe the mechanisms behind metastatic invasion: one can manipulate the cells, vary the composition or density of the extracellular matrix, add other secondary cell types, and add any number of soluble factors or pharmacologic inhibitors to the overlying culture medium. More generally, the ability to evaluate the end point of invasion quantitatively in all four dimensions of any tumor line allow the experimentalist concrete end points to determine the statistical significance between experimental conditions.

We anticipate that this system will be most useful as a cost-effective, high-throughput screening tool to assess the effect of pharmacologic inhibitors and microenvironmental cues (perhaps synergistically) on the invasive capacity of tumor cells at a metastatic site, arming researchers with another means to validate therapies in an appropriate setting before advancing to more costly *in vivo* studies.

Acknowledgments

We thank Katherine Blevins and Dr. Zifu Wang for technical assistance.

References

1. Sporn MB. The war on cancer. Lancet 1996;347:1377–81.

2. Miller AJ, Mihm MC, Jr. Melanoma. N Engl J Med 2006;355:51–65.

3. Postovit LM, Seftor EA, Seftor RE, Hendrix MJ. Influence of the microenvironment on melanoma cell fate determination and phenotype. Cancer Res 2006;66:7833–6.

4. Jemal A, Siegel R, Ward E, et al. Cancer statistics, 2006. CA Cancer J Clin 2006;56:106–30.

5. Lee JT, Herlyn M. Embryogenesis meets tumorigenesis. Nat Med 2006;12:882–4.

6. Bittner M, Meltzer P, Chen Y, et al. Molecular classification of cutaneous malignant melanoma by gene expression profiling. Nature 2000;406:536–40.

7. Hoek K, Rimm DL, Williams KR, et al. Expression profiling reveals novel pathways in the transformation of melanocytes to melanomas. Cancer Res 2004;64:5270–82.

8. Hoek KS, Schlegel NC, Brafford P, et al. Metastatic potential of melanomas defined by specific gene expression profiles with no BRAF signature. Pigment Cell Res 2006;19:290–302.

9. Smith AP, Hoek K, Becker D. Whole-genome expression profiling of the melanoma progression pathway reveals marked molecular differences between nevi/melanoma *in situ* and advanced-stage melanomas. Cancer Biol Ther 2005;4:1018–29.

10. Ruiter D, Bogenrieder T, Elder D, Herlyn M. Melanoma-stroma interactions: structural and functional aspects. Lancet Oncol 2002;3:35–43.

11. Seftor EA, Brown KM, Chin L, et al. Epigenetic transdifferentiation of normal melanocytes by a metastatic melanoma microenvironment. Cancer Res 2005;65:10164–9.

12. Topczewska JM, Postovit LM, Margaryan NV, et al. Embryonic and tumorigenic pathways converge via nodal signaling: role in melanoma aggressiveness. Nat Med 2006;12:925–32.

13. Soengas MS, Lowe SW. Apoptosis and melanoma chemoresistance. Oncogene 2003;22:3138–51.

14. Steeg PS. Tumor metastasis: mechanistic insights and clinical challenges. Nat Med 2006;12:895–904.

15. MacDonald IC, Groom AC, Chambers AF. Cancer spread and micrometastasis development: quantitative approaches for *in vivo* models. Bioessays 2002;24:885–93.

16. Hendrix MJ, Gehlsen KR, Wagner HN, Jr., Rodney SR, Misiorowski RL, Meyskens FL, Jr. *In vitro* quantification of melanoma tumor cell invasion. Clin Exp Metastasis 1985;3:221–33.

17. Albini A, Iwamoto Y, Kleinman HK, et al. A rapid *in vitro* assay for quantitating the invasive potential of tumor cells. Cancer Res 1987;47:3239–45.

18. Ghajar CM, Blevins KS, Hughes CC, George SC, Putnam AJ. Mesenchymal stem cells enhance angiogenesis in mechanically viable prevascularized tissues via early matrix metalloproteinase upregulation. Tissue Eng 2006;12:2875–88.

19. Welch DR, Chen P, Miele ME, et al. Microcell-mediated transfer of chromosome 6 into metastatic human C8161 melanoma cells suppresses metastasis but does not inhibit tumorigenicity. Oncogene 1994;9:255–62.

20. Bregman MD, Meyskens FL, Jr. Difluoromethylornithine enhances inhibition of melanoma cell growth in soft agar by dexamethasone, clone A interferon and retinoic acid. Int J Cancer 1986;37:101–7.

21. Welch DR, Bisi JE, Miller BE, et al. Characterization of a highly invasive and spontaneously metastatic human malignant melanoma cell line. Int J Cancer 1991;47:227–37.

22. Katano M, Saxton RE, Cochran AJ, Irie RF. Establishment of an ascitic human melanoma cell line that metastasizes to lung and liver in nude mice. J Cancer Res Clin Oncol 1984;108:197–203.

23. Dvorak HF, Senger DR, Dvorak AM. Fibrin as a component of the tumor stroma: origins and biological significance. Cancer Metastasis Rev 1983;2:41–73.

24. Brown LF, Asch B, Harvey VS, Buchinski B, Dvorak HF. Fibrinogen influx and accumulation of cross-linked fibrin in mouse carcinomas. Cancer Res 1988;48:1920–5.

25. Houghton AN, Polsky D. Focus on melanoma. Cancer Cell 2002;2:275–8.

26. Friedl P, Wolf K. Tumour-cell invasion and migration: diversity and escape mechanisms. Nat Rev Cancer 2003;3:362–74.

27. Palumbo JS, Kombrinck KW, Drew AF, et al. Fibrinogen is an important determinant of the metastatic potential of circulating tumor cells. Blood 2000;96:3302–9.

28. Biggerstaff JP, Seth N, Amirkhosravi A, et al. Soluble fibrin augments platelet/tumor cell adherence *in vitro* and *in vivo* and enhances experimental metastasis. Clin Exp Metastasis 1999;17:723–30.

29. Collen A, Hanemaaijer R, Lupu F, et al. Membrane-type matrix metalloproteinase-mediated angiogenesis in a fibrin-collagen matrix. Blood 2003;101:1810–7.

30. Kalluri R, Zeisberg M. Fibroblasts in cancer. Nat Rev Cancer 2006;6:392–401.

31. Li G, Satyamoorthy K, Meier F, Berking C, Bogenrieder T, Herlyn M.

Function and regulation of melanoma-stromal fibroblast interactions: when seeds meet soil. Oncogene 2003;22:3162 – 71.

32. Bootle-Wilbraham CA, Tazzyman S, Marshall JM, Lewis CE. Fibrinogen E-fragment inhibits the migration and tubule formation of human dermal microvascular endothelial cells *in vitro*. Cancer Res 2000;60: 4719 – 24.

33. Weitz JI, Leslie B, Ginsberg J. Soluble fibrin degradation products potentiate tissue plasminogen activator-induced fibrinogen proteolysis. J Clin Invest 1991;87:1082 – 90.

34. Stack S, Gonzalez-Gronow M, Pizzo SV. Regulation of plasminogen activation by components of the extracellular matrix. Biochemistry 1990; 29:4966 – 70.

35. Meier F, Nesbit M, Hsu MY, et al. Human melanoma progression in skin reconstructs: biological significance of bFGF. Am J Pathol 2000;156: 193 – 200.

36. Herlyn M. Metastatic melanoma cells. Introduction. Cancer Metastasis Rev 2005;24:193 – 4.

37. Debnath J, Brugge JS. Modelling glandular epithelial cancers in three-dimensional cultures. Nat Rev Cancer 2005;5:675 – 88.

38. Ghosh S, Spagnoli GC, Martin I, et al. Three-dimensional culture of melanoma cells profoundly affects gene expression profile: a high density oligonucleotide array study. J Cell Physiol 2005;204:522 – 31.

39. Weaver VM, Fischer AH, Peterson OW, Bissell MJ. The importance of the microenvironment in breast cancer progression: recapitulation of mammary tumorigenesis using a unique human mammary epithelial cell model and a three-dimensional culture assay. Biochem Cell Biol 1996;74: 833 – 51.

40. Satyamoorthy K, Meier F, Hsu MY, Berking C, Herlyn M. Human xenografts, human skin and skin reconstructs for studies in melanoma development and progression. Cancer Metastasis Rev 1999;18:401 – 5.